Supplement of Atmos. Meas. Tech., 18, 3051–3072, 2025
https://doi.org/10.5194/amt-18-3051-2025-supplement

Atmospheric Measurement Techniques
Open Access

Supplement of

Development and validation of a NO_x^+ ratio method for the quantitative separation of inorganic and organic nitrate aerosol using a unit-mass-resolution time-of-flight aerosol chemical speciation monitor equipped with a capture vaporizer (CV-UMR-ToF-ACSM)

Farhan R. Nursanto et al.

Correspondence to: Farhan R. Nursanto (farhan.nursanto@wur.nl) and Juliane L. Fry (juliane.fry@wur.nl)

S1 Revised fragmentation table development

The revised CV-UMR-ToF-ACSM fragmentation table development is based on catalogued and newly collected CV-HR-ToF-AMS and CV-UMR-ToF-ACSM mass spectra. The CV-HR-ToF-AMS mass spectra are retrieved from the AMS spectral database (Hu et al., http://cires1.colorado.edu/jimenez-group/AMSsd_CV, last access: 9 July 2025), where a variety of nitrate-containing and non-nitrate organic aerosol (OA) were measured (see Tables S1 and S2).

Table S1. Summary of CV-HR-ToF-AMS mass spectra (both V-mode and W-mode) from the AMS spectral database used to obtain correlations between Org fragment mass. The organic aerosol (OA) spectra originated from chamber experiments, ambient, and laboratory measurements from different studies. The vaporizer temperature (T_{CV}) is also specified.

Type	ID	Description	Citation	T_{CV} (°C)	Campaign/location/time
Chamber experiment	001	SOA from α-pinene + O_3 in dark chamber chemistry (pinene+O_3)	Hu et al. (2018a)	600	CU chambers, CU campus (Boulder, CO, US)
	002	SOA from 100 ppb δ-carene + NO_3 (carene+NO_3)	Hu et al. (2018a)	600	
	003	SOA from 100 ppb α-pinene + NO_3 + $(NH_4)_2SO_4$ seed (pinene+NO_3+SO_4)	Hu et al. (2018a)	600	
Ambient positive matrix factorization (PMF) factor	001	Cooking OA (COA)	Hu et al. (2017)	525	Boulder study, CU campus (Boulder, CO, US, April 2013)
	002	Hydrocarbon-like OA (HOA)	Hu et al. (2017)	525	
	003	Oxygenated OA (OOA)	Hu et al. (2017)	525	
	008	Isoprene epoxydiols-derived SOA (IEPOX-SOA)	Hu et al. (2018b)	550	SOAS campaign (Centreville, AL, US, June-July 2013)
	012	More-oxidized oxygenated OA (MO-OOA)	Hu et al. (2018b)	600	KORUS-AQ study (RF05) flight (Seoul, South Korea, May 2016)
	013	Less-oxidized oxygenated OA (LO-OOA)	Hu et al. (2018b)	600	
	014	Hydrocarbon-like OA (HOA)	Hu et al. (2018b)	600	
Laboratory OA/SOA	001	Acetyl salicylic acid (AcSal-H, $C_9H_8O_4$)	Hu et al. (2018b)	600	CU laboratory, CU campus (Boulder, CO, US)
	002	Folic acid (folic-H, $C_{19}H_{19}N_7O_6$)	Hu et al. (2018b)	600	
	006	Caffeine ($C_8H_{10}N_4O_2$)	Hu et al. (2018b)	600	
	007	Histidine (His, $C_6H_9N_3O_2$)	Hu et al. (2018b)	600	
	008	Tryptophan (Try, $C_{11}H_{12}N_2O_2$)	Hu et al. (2018b)	600	
	010	Nicotinic acid (nicotinic-H, $C_6H_5NO_2$)	Hu et al. (2018b)	600	
	011	Sucrose (sucrose_1, $C_{12}H_{22}O_{11}$)	Hu et al. (2018b)	600	
	015	Oleic acid (oleic-H_1, $C_{18}H_{34}O_2$)	Hu et al. (2018b)	600	
	016	Squalene (squalene_1, $C_{30}H_{50}$)	Hu et al. (2018b)	600	
	018	Bis-(2-ethylhexyl)-ester (bis(2-EtHex)ester, $C_{26}H_{50}O_4$)	Hu et al. (2018a)	600	
	020	Oleic acid (oleic-H_2, $C_{18}H_{34}O_2$)	Hu et al. (2018a)	600	
	021	Squalene (squalene_2, $C_{30}H_{50}$)	Hu et al. (2018a)	600	
	023	Glutaric acid (glutaric-H, $C_5H_8O_4$)	Hu et al. (2018a)	600	
	024	Octacosane ($C_{28}H_{58}$)	Hu et al. (2018a)	550	
	026	Sucrose (sucrose_2, $C_{12}H_{22}O_{11}$)	Hu et al. (2018a)	600	

The chamber experiment spectra were obtained from CU Atmospheric Chamber facility (Boulder, Colorado, United States, see Hu et al. (2018a)). The ambient PMF factors were measured at different locations: three spectra at the University of Colorado during spring (Boulder, Colorado, United States, (Hu et al., 2017)), one spectrum from SOAS campaign at a pollution-influenced forest site during summer (Centreville, Alabama, United States, (Carlton et al., 2018; Hu et al., 2018b)), and three spectra from an aircraft-based field campaign as part of KORean-United States Air Quality mission (KORUS-AQ, https://espo.nasa.gov/home/korus-aq, last access: 9 July 2025). The laboratory standard measurements account for 15 mass spectra, ranging from carboxylic acids, hydrocarbons, nitrogen-containing compounds, and amino acids. Table S1 lists all of the OA datasets used, including both experiments containing and not containing nitrate.

The CV-UMR-ToF-ACSM mass spectra measured in chamber experiments when there is no or negligible nitrate present are summarized in Table S2. Because these are UMR spectra, we cannot use any experiments that contained nitrate. Therefore, the investigated nominal masses are assumed to contain only Org fragments (m/z 29, m/z 30, m/z 42, m/z 43, m/z 45, m/z 46). The chamber experiments were conducted in Aerosol Interaction and Dynamics in the Atmosphere (AIDA) chamber, a facility maintained by Institute of Meteorology and Climate Research (IMK) in Karlsruhe Institute of Technology (KIT), Germany. The experiments were part of the Cloud-Aerosol Interactions in a Nitrogen-dominated Atmosphere (CAINA) project (https://sites.google.com/view/cainaproject/, last access: 9 July 2025).

Table S2. Summary of CV-UMR-ToF-ACSM mass spectra from nitrate-free chamber experiments used to obtain correlations between Org fragment mass. The mass spectra are measured using ACSM-RUG with vaporizer temperature (T_{CV}) of 525 °C.

Type	ID	Description	Campaign/location/time
Chamber experiment	004	SOA from isoprene + O_3 + TME + $(NH_4)_2SO_4$ seed in dark chamber (isoprene+O_3+TME(+AmS))	AIDA chamber, IMK KIT (Karslruhe, DE)
	005	SOA from α-pinene + O_3 + TME + NaCl seed in dark chamber (pinene+O_3+TME(+NaCl))	
	006	SOA from glyoxal + $(NH_4)_2SO_4$ seed in dark chamber (glyoxal(+AmS)_1)	
	007	SOA from glyoxal + NaCl seed in dark chamber (glyoxal(+NaCl)_1)	
	008	SOA from glyoxal + $(NH_4)_2SO_4$ seed in dark chamber (glyoxal(+AmS)_2)	
	009	SOA from glyoxal + NaCl seed in dark chamber (glyoxal(+NaCl)_2)	

The slope of the orthogonal distance regression (ODR) fits to determine the multiplier $a_{\mathrm{Org[30],[}i\mathrm{]}}$ and $a_{\mathrm{Org[46],[}i\mathrm{]}}$ using the simulated UMR spectra (of the HR dataset) and UMR dataset are summarized in Table S3. The uncertainty of the value from the fit slope is also included. To confirm the best fit of the multipliers, the predicted UMR mass (calculated using the multiplier) is compared to the measured UMR mass (sum of mass measured in original spectra) which is resumed in Table S4.

Table S3. Summary of the ODR fit parameters with intercept at zero between different UMR nominal mass to predict (frag_Org[x]) and related UMR nominal mass (frag_Org[i]) from the full dataset (frag_Org[x] = $a_{\mathrm{Org[}x\mathrm{],[i]}}$ · frag_Org[i]). The slope is defined as the multiplier $a_{\mathrm{Org[}x\mathrm{],[i]}}$ which defines the fractional relation between the two UMR masses investigated.

UMR mass to predict (x)	frag_Org[30] = $a_{\mathrm{Org[30],[i]}}$ · frag_Org[i]			frag_Org[46] = $a_{\mathrm{Org[46],[i]}}$ · frag_Org[i]		
UMR daughter mass (i)	$a_{\mathrm{Org[CH_2O^+],[i]}} \pm s_a$	r^2	χ^2	$a_{\mathrm{Org[CH_4NO^+],[i]}} \pm s_a$	r^2	χ^2
frag_Org[29]	**0.311 ± 0.016**	**0.88**	1.57E-3	(3.17 ± 2.49)E-3	0.11	4.27E-5
frag_Org[42]	0.963 ± 0.230	0.05	0.01	0.024 ± 0.006	0.01	3.06E-5
frag_Org[43]	0.367 ± 0.108	0.01	0.02	0.012 ± 0.004	1.70E-3	3.54E-5
frag_Org[45]	14.002 ± 3.559	0.02	2.33E-4	**0.305 ± 0.037**	**0.43**	1.35E-5

i represent masses related to frag_Org[30] (i.e., $C^{18}O^+$, $^{13}CHO^+$, CH_2O^+, CH_4N^+, $^{13}CH_3N^+$, $^{13}CCH_5^+$, $C_2H_6^+$) and frag_Org[46] (i.e., $C^{18}OO^+$, $^{13}CHO_2^+$, $CH_2O_2^+$, $^{13}CH_3NO^+$, CH_4NO^+, $^{13}CCH_5O^+$, $C_2H_6O^+$) tested in this study. It includes frag_Org[29] (i.e., $^{13}CO^+$, CHO^+, CH_3N^+, $C_2H_5^+$), frag_Org[42] (i.e., $^{13}CCHO^+$, $C_2H_2O^+$, $C_2H_4N^+$, $C_2H_3^{15}N^+$, $^{13}CCH_3N^+$, $C_2H4_N^+$, $^{13}CC_2H_5^+$, $C_3H_6^+$), frag_Org[43] (i.e., $CHNO^+$, $^{13}CCH_2O^+$, $C_2H_3O^+$, $C_2H_4^{15}N^+$, $^{13}CCH_4N^+$, $C_2H_5N^+$, $^{13}CC_2H_6^+$, $C_3H_7^+$), and frag_Org[45] (i.e., $^{13}CO_2^+$, CHO_2^+, $^{13}CH_2NO^+$, CH_3NO^+, $^{13}CCH_4O^+$, $C_2H_5O^+$, $^{13}CCH_6N^+$, $C_2H_7N^+$, $^{13}C_2CH_7^+$, $^{13}CC_2H_8^+$). The choice is based on the list studied in Fry et al. (2018).

$a_{\mathrm{Org[}x\mathrm{],[}i\mathrm{]}}$ is the coefficient for frag_Org[x] component, obtained from the slope of linear regression fit between frag_Org[x] and frag_Org[i]. Values printed in **bold** represent the best correlation for frag_Org[x].

Table S4. The multipliers $a_{\mathrm{Org}[x],[\mathrm{i}]} \cdot$ frag_Org[i] for frag_Org[30] and frag_Org[46] from this study and other studies, re-applied to the simulated UMR spectra from the HR and UMR datasets.

Work	$a_{\mathrm{Org}[30],[29]}$	r^2 (a)	χ^2 (a)	Predicted/ measured(b)	$a_{\mathrm{Org}[46],[45]}$	r^2 (a)	χ^2 (a)	Predicted/ measured(b)
	frag_Org[30] = $a_{\mathrm{Org}[30],[29]} \cdot$ frag_Org[29]				frag_Org[46] = $a_{\mathrm{Org}[46],[45]} \cdot$ frag_Org[45]			
this study (CV-ToF)(c)	**0.311±0.016**	0.88	8.48E-4	**(96.9±4.9)%**	**0.305±0.037**	0.43	6.79E-6	**(82.5±9.5)%**
Allan et al. (2004) (default)	0.022	0.88	8.03E-6	(6.6±3.4)%	-	-	-	-
Fry et al. (2018) (SV-ToF)	0.215	0.88	5.40E-4	(66.0±3.3)%	0.127	0.43	1.71E-6	(30.3±3.7)%
Hu et al. (2017) (biogenic, SV-ToF)	0.31	0.88	8.44E-4	(96.4±4.8)%	0.42	0.43	9.34E-6	(121.7±14.0)%
Hu et al. (2017) (biogenic, CV-ToF)	0.32	0.88	8.71E-4	(99.7±5.0)%	0.68	0.43	1.22E-5	(214.4±25.5)%

(a) the coefficient of determination (r^2) and chi-squared (χ^2) values refer to the slope of ODR fit used to obtain the values of $a_{\mathrm{Org}[x],[\mathrm{i}]}$.

(b) data from CV-ToF-AMS spectral database and experiments in AIDA chamber described in Table S1 and S2, fit for typical ambient dataset. Values printed in **bold** represent the best correlation for frag_Org[x]. The value in percentage is reported with $\pm 2\sigma$.

(c) predicted UMR frag_Org[x] (calculated from dataset spectra, frag_Org[x] = $a_{\mathrm{Org}[x],[\mathrm{i}]}$*frag_Org[$i$]) vs measured frag_Org[$x$] (sum of all Org fragments in the nominal m/z x of the original dataset spectra).

We also explore different multipliers that are compatible for different composition profile. We perform the ODR fit of frag_Org[30] against frag_Org[29], and frag_Org[46] against frag_Org[45] to chamber experiment spectra that use glyoxal and terpenes (e.g., isoprene, limonene) as precursor to obtain composition-specific fragmentation table for each (see Fig. S1).

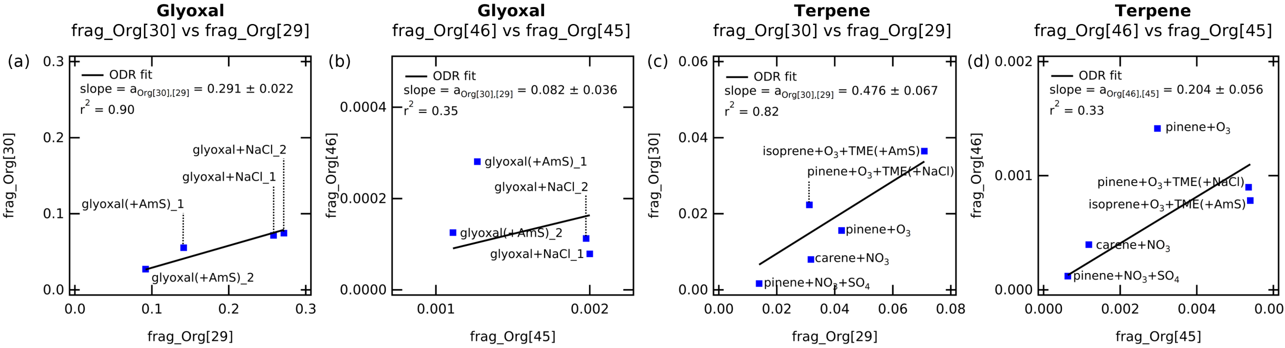

Figure S1. The ODR fits (set to zero intercept) to determine the multipliers $a_{\mathrm{Org}[x],[i]}$ for composition-specific fragmentation table of (a,b) glyoxal and (c,d) terpene. The ODR fits show the correlation between the signals of (a,c) frag_Org[30] vs frag_Org[29], and (b,d) frag_Org[46] vs frag_Org[45].

Higher uncertainty shows more variability of organic fragment composition that leads to uncertainties for frag_NO_3[30] and frag_NO_3[46], which later affect the calculation of observed NO_x^+ ratio (R_{obs}) and mass fraction of NO_3 existing as particulate organic nitrate (f_{pON}).

S2 Summary of experimental R_{pAmN} of CV-UMR-ToF-ACSM

The measurements of R_{pAmN} from two CV-UMR-ToF-ACSM instruments used in the main article are summarized in Table S5.

Table S5. Summary of measured $\mathrm{NO_x^+}$ ratio of particulate ammonium nitrate (R_{pAmN}) from two CV-UMR-ToF-ACSM in the Netherlands, as part of routine calibration measurements. The uncertainty on each measurement is included. The value is obtained by performing ODR fits to zero intercept of the signal of m/z 46 against m/z 30 (no fragmentation table applied). The instruments are part of the Ruisdael Observatory monitoring site network in the Netherlands managed by different institutions: ACSM-UU by Utrecht University (UU) and ACSM-RUG by University of Groningen (RUG).

Location	Date (dd/mm/yyyy)	$R_{\mathrm{pAmN}} \pm s_{\mathrm{R}}$	r^2	χ^2
ACSM UU				
CESAR tower, Cabauw, Netherlands	09/04/2021	0.0227 ± 0.0005	0.94	7.54E-4
CESAR tower, Cabauw, Netherlands	16/04/2021	0.0233 ± 0.0005	0.98	9.47E-4
CESAR tower, Cabauw, Netherlands	27/07/2021	0.0253 ± 0.0003	0.99	2.47E-3
CESAR tower, Cabauw, Netherlands	14/04/2023	0.0232 ± 0.0002	0.99	3.56E-2
LSCE CEA Paris-Saclay, France	14/11/2023	0.0241 ± 0.0001	0.99	5.27E-2
	Mean	**0.0237 ± 0.0009**		
ACSM RUG				
Lutjewad, Groningen, Netherlands	08/03/2023	0.0114 ± 0.0002	0.98	3.75E-3
LSCE CEA Paris-Saclay, France	16/11/2023	0.0116 ± 0.0002	0.99	3.17E-3
AIDA chamber IMK KIT, Karlsruhe, Germany	09/01/2024	0.0112 ± 0.0001	0.99	1.88E-3
	Mean	**0.0114 ± 0.0002**		

S3 "Excess $\mathrm{NH_4}$" method to determine lower limit of R_{pON} from chamber experiment

The values of $\mathrm{NO_x^+}$ ratio of particulate organic nitrate (R_{pON}) in this study are determined from an AIDA chamber experiment at IMK KIT, Karlsruhe, Germany. The experiment, described in Section 4.2 of the main text, used glyoxal as an SOA precursor, reacted with $\mathrm{NO_3}$ (from $\mathrm{NO_2}$ and $\mathrm{O_3}$), and used NaCl seed. The average $\mathrm{NO_x^+}$ ratio observed during particulate organic nitrate (pON) formation is taken as R_{pON} if we assume all nitrate aerosol formed is pON from the reaction of $\mathrm{NO_3}$ with glyoxal.

However, chamber experiments can contain impurities, for example, inorganic nitrate can also be formed from $\mathrm{HNO_3}$ uptake or repartitioning of semi-volatile $\mathrm{NH_4NO_3}$ from the chamber walls during pON formation. Therefore, it may not produce pure pON and the $\mathrm{NO_x^+}$ ratio observed cannot necessarily be assumed to be R_{pON}. By removing the inorganic nitrate impurities through "excess $\mathrm{NH_4}$" method (Takeuchi and Ng, 2019), we define R_{pON} as the lower limit of R_{pON} because it represents the lowest possible $\mathrm{NO_x^+}$ ratio.

The "excess $\mathrm{NH_4}$" method is a way to estimate the inorganic nitrate contribution to the total $\mathrm{NO_3}$ based on the increase in $\mathrm{NH_4}$. It assumes that any increase in $\mathrm{NH_4}$ during aerosol growth is entirely due to $\mathrm{NH_4NO_3}$ formation (molar concentration of excess $\mathrm{NH_4}$ = molar concentration of inorganic nitrate). From there, we can subtract this maximum inorganic nitrate mass from the total $\mathrm{NO_3}$ to determine f_{pON}. By having information on f_{pON}, $\mathrm{NO_x^+}$ ratio of particulate ammonium nitrate (R_{pAmN}), and observed $\mathrm{NO_x^+}$ ratio (R_{obs}), we are able to determine the value of R_{pON} of any purity level of pON formation by rearranging Eq. S1 (Farmer et al., 2010) into Eq. S2.

$$f_{\mathrm{pON}} = \frac{(R_{\mathrm{obs}} - R_{\mathrm{pAmN}})(1 + R_{\mathrm{pON}})}{(R_{\mathrm{pON}} - R_{\mathrm{pAmN}})(1 + R_{\mathrm{obs}})} \tag{S1}$$

$$R_{\mathrm{pON}} = \frac{(R_{\mathrm{obs}} \cdot R_{\mathrm{pAmN}} \cdot f_{\mathrm{pON}}) + R_{\mathrm{obs}} + (R_{\mathrm{pAmN}} \cdot f_{\mathrm{pON}}) - R_{\mathrm{pAmN}}}{(R_{\mathrm{obs}} \cdot f_{\mathrm{pON}}) - R_{\mathrm{obs}} + R_{\mathrm{pAmN}} + f_{\mathrm{pON}}} \tag{S2}$$

We consider this to be the highest estimate of the potential inorganic nitrate interference, because all $\mathrm{NH_4}$ is not necessarily $\mathrm{NH_4NO_3}$. For example, there can be $\mathrm{NH_4Cl}$ formed since in this experiment we have NaCl seed aerosol.

S4 Propagation of uncertainty

The value of f_{pON} is calculated from measurements that contain uncertainties as part of its measurement (see Eq. S1). In this section, we describe in detail how the uncertainty is propagated from different measurements acquired using the UMR instrument and fragmentation table, or HR instrument and peak fitting, into f_{pON}. Overall, the uncertainties for f_{pON} are sourced from 3 main parameters, which are the $\mathrm{NO_x^+}$ ratio of the observed air (R_{obs}), pure ammonium nitrate (R_{pAmN}), and pure organic nitrate (R_{pON}). Each ratio itself is calculated from values containing uncertainties. In this work, the uncertainty is propagated from the standard error ($s_{\overline{x}}$) of the sample (Eq. S3).

$$s_{\overline{x}} = \frac{s}{\sqrt{N}} = \frac{1}{\sqrt{N}} \cdot \sqrt{\frac{1}{N-1}\sum_{i=1}^{N}(x_i - \overline{x})^2} \tag{S3}$$

x_i : data point i of variable x

$\overline{x}$: mean of data points

N : number of data points.

S4.1 R_{obs}

For UMR measurements, R_{obs} is calculated using observed signals ($C_{\mathrm{NO^+}}$ and $C_{\mathrm{NO_2^+}}$) measured while sampling ambient or chamber generated particles, as described in the revised fragmentation table (see Table 4), rewritten in Eq. S4 below,

$$R_{\mathrm{obs}} = \frac{(C_{\mathrm{NO_2^+}})_{\mathrm{obs}}}{(C_{\mathrm{NO^+}})_{\mathrm{obs}}} = \frac{C_{[46]} - a_{\mathrm{Org[46],[45]}} \cdot C_{[45]}}{C_{[30]} - a_{\mathrm{Org[30],[29]}} \cdot C_{[29]}}. \tag{S4}$$

Therefore, R_{obs} contains in total of six uncertainty terms. Four uncertainty sources originated from the measured signals of $m/z\ x$ ($C_{[x]}$, x = [29,30,45,46]). The uncertainty is generated by Tofware v3.3, which is described as being calculated based on ion counting statistics and an estimated electronic noise of the instrument.

The other two uncertainties come from the multipliers $a_{\mathrm{Org[30],[29]}}$ and $a_{\mathrm{Org[46],[45]}}$ represented by the uncertainty of ODR fits described in Table S3. While the uncertainty from concentrations or signals varies over the course of time, the uncertainty from the multipliers remains constant. The propagated uncertainty of R_{obs} ($s_{\overline{R}_{\mathrm{obs}}}$) , see Eq. S7) is calculated from the uncertainty of $\mathrm{NO_2^+}$ signal ($s_{\overline{C}_{\mathrm{NO_2^+}}}$), see Eq. S5) and $\mathrm{NO^+}$ signal ($s_{\overline{C}_{\mathrm{NO^+}}}$)), see Eq. S6),

$$s_{\overline{C}_{\mathrm{NO_2^+}}} = \sqrt{(s_{\overline{C}_{[46]}})^2 + \left(a_{\mathrm{Org[46],[45]}} \cdot C_{[45]} \cdot \sqrt{\left(\frac{s_{\overline{a}_{\mathrm{Org[46],[45]}}}}{a_{\mathrm{Org[46],[45]}}}\right)^2 + \left(\frac{s_{(\overline{C}_{[45]})}}{C_{[45]}}\right)^2}\right)^2} \tag{S5}$$

$$s_{\overline{C}_{\mathrm{NO^+}}} = \sqrt{(s_{(\overline{C}_{[30]})})^2 + \left(a_{\mathrm{Org[30],[29]}} \cdot C_{[29]} \cdot \sqrt{\left(\frac{s_{\overline{a}_{\mathrm{Org[30],[29]}}}}{a_{\mathrm{Org[30],[29]}}}\right)^2 + \left(\frac{s_{\overline{C}_{[29]}}}{C_{[29]}}\right)^2}\right)^2} \tag{S6}$$

$$s_{\overline{R}_{\mathrm{obs}}} = R_{\mathrm{obs}} \cdot \sqrt{\left(\frac{s_{\overline{C}_{\mathrm{NO^+}}}}{C_{\mathrm{NO^+}}}\right)^2 + \left(\frac{s_{\overline{C}_{\mathrm{NO_2^+}}}}{C_{\mathrm{NO_2^+}}}\right)^2}. \tag{S7}$$

For HR measurements, the $\mathrm{NO^+}$ and $\mathrm{NO_2^+}$ signal contributions are obtained through HR peak fitting using PIKA module of ToF-AMS HR Analysis 1.26E. Therefore, $s_{\overline{C}_{\mathrm{NO^+}}}$ and $s_{\overline{C}_{\mathrm{NO_2^+}}}$ are simply the peak fitting uncertainties output by PIKA.

S4.2 R_{pAmN} and R_{pON}

As it is typical to measure particulate ammonium nitrate (pAmN) as part of the AMS/ACSM instrument calibration, we propagate the uncertainty of R_{pAmN} from repeated NH_4NO_3 calibration ($s_{\overline{R}_{\text{pAmN}}}$, see Eq. S8). It thus represents how much the instrument's response to pAmN diverges over the course of time. Therefore, R_{pAmN} contributes in total to one uncertainty term and is constant for each time point.

$$s_{\overline{R}_{\text{pAmN}}} = \frac{1}{\sqrt{N}} \cdot \sqrt{\frac{1}{N-1}\sum_{i=1}^{N}(R_{\text{pAmN}_i} - \overline{R}_{\text{pAmN}})^2} \tag{S8}$$

R_{pAmN_i} : calculated R_{pAmN} value from measurement i

$\overline{R}_{\text{pAmN}}$: average R_{pAmN} value

N : number of repeated pAmN measurements.

In this study, we omit the uncertainty of R_{pON} ($s_{\overline{R}_{\text{pON}}}$) from the propagation. Instead, the uncertainty of R_{pON} is obtained through the calculation of f_{pON} using the lower and upper limit of R_{pON} described in Section 4.2. By combining the propagation of uncertainty and the range of R_{pON}, the final uncertainty will include R_{obs}, R_{pAmN}, and R_{pON}.

S4.3 Propagation of uncertainty to the final function

The uncertainty is propagated as standard error from each variable, calculated using a simplified approach described in Eqs. S9 and S10. This approach is used because R_{obs} and R_{pAmN} appear several times in Eq. S1 to calculate f_{pON}. If we use the standard rule of uncertainty propagation, it will result in multiple representations of the same uncertainty in the calculation, which will lead to a higher propagated uncertainty. Simplified uncertainty propagation assumes independent, uncorrelated variables to yield a common function formula. The propagated uncertainty in the form of standard error of the function (s_f) is derived from the standard error (s_{x_i}) and the partially derived function ($\frac{\partial f}{\partial x_i}$) for each variable or uncertainty source, as defined by Eq. S9. The formula is applied to f_{pON} and gives the final uncertainty propagation equation as shown in Eq. S10, S11, S12, and S13.

$$s_{f(x_i,x_{i+1},...)} = \sqrt{\sum_{i=1}^{N}\left(\frac{\partial f(x_i,x_{i+1},...)}{\partial x_i}\right)^2 \cdot s_{x_i}^2} \tag{S9}$$

$$s_{f_{\text{pON}}} = \sqrt{\left(\frac{\partial f_{\text{pON}}}{\partial R_{\text{obs}}}\right)^2 \cdot s_{\overline{R}_{\text{obs}}}^2 + \left(\frac{\partial f_{\text{pON}}}{\partial R_{\text{pAmN}}}\right)^2 \cdot s_{\overline{R}_{\text{pAmN}}}^2 + \left(\frac{\partial f_{\text{pON}}}{\partial R_{\text{pON}}}\right)^2 \cdot s_{\overline{R}_{\text{pON}}}^2} \tag{S10}$$

By taking f_{pON} from Eq. S1, the partial derivatives are as follows:

$$\frac{\partial f_{\text{pON}}}{\partial R_{\text{obs}}} = \frac{(R_{\text{pAmN}}+1)\cdot(R_{\text{pON}}+1)}{(R_{\text{obs}}+1)^2\cdot(R_{\text{pON}}-R_{\text{pAmN}})} \tag{S11}$$

$$\frac{\partial f_{\text{pON}}}{\partial R_{\text{pAmN}}} = \frac{(R_{\text{obs}}-R_{\text{pON}})\cdot(R_{\text{pON}}+1)}{(R_{\text{obs}}+1)\cdot(R_{\text{pON}}-R_{\text{pAmN}})^2} \tag{S12}$$

$$\frac{\partial f_{\text{pON}}}{\partial R_{\text{pON}}} = \frac{(-R_{\text{pAmN}}-1)\cdot(R_{\text{obs}}-R_{\text{pAmN}})}{(R_{\text{obs}}+1)\cdot(R_{\text{pON}}-R_{\text{pAmN}})^2} \tag{S13}$$

To propagate the uncertainty further into concentration, we combine the final uncertainty of f_{pON} and the total concentration of nitrate ($C_{\text{pNO}_3\text{,tot}}$) generated from Tofware v3.3 ($s_{\overline{C}_{\text{pNO}_3\text{,tot}}}$), using Eqs. S14 and S15. The uncertainty of f_{pAmN} can be assumed to be equal to that of f_{pON} due to their relationship (f_{pON} + f_{pAmN} = 1).

$$s_{\overline{C}_{\text{pON}}} = C_{\text{pNO}_3\text{,tot}} \cdot f_{\text{pON}} \cdot \sqrt{\left(\frac{s_{\overline{C}_{\text{pNO}_3\text{,tot}}}}{C_{\text{pNO}_3\text{,tot}}}\right)^2 + \left(\frac{s_{\overline{f}_{\text{pON}}}}{f_{\text{pON}}}\right)^2} \tag{S14}$$

$$s_{\overline{C}_{\text{pAmN}}} = C_{\text{pNO}_3\text{,tot}} \cdot f_{\text{pAmN}} \cdot \sqrt{\left(\frac{s_{\overline{C}_{\text{pNO}_3\text{,tot}}}}{C_{\text{pNO}_3\text{,tot}}}\right)^2 + \left(\frac{s_{\overline{f}_{\text{pAmN}}}}{f_{\text{pAmN}}}\right)^2}. \tag{S15}$$

Note that the reported uncertainties are related to precision uncertainty only. Additional uncertainties associated with C_{pNO_3} concentration quantification (e.g. ionization efficiency, flow rate correction) are not included here to highlight values and trends in the apportionment. These uncertainties were estimated to be ±34% for 2σ using an SV-AMS by Bahreini et al. (2009). We might expect the uncertainty to be even smaller when using a CV due reduced uncertainties from collection efficiency effects.

S5 Positive matrix factorization (PMF) analysis to the CV-UMR-ToF-ACSM measurements

In this section, we describe the PMF analysis applied to the chamber experiment using limonene precursor described in Section 6.2. The larger picture of the experiment is shown in Fig. S2a,b. The PMF analysis to the CV-UMR-ToF-ACSM measurements only cover the indicated red square of the time series, where it is compared to the NO_x^+ ratio method in Section 6.2.

The 2 min average matrices of UMR organic fragment mass spectra with a m/z of 12 to 120, fragments of ammonium (NH_4_16 and NH_4_17, two main signals of NH_4 which are NH_2^+ and NH_3^+), and fragments of nitrate (NO_3_30 and NO_3_46, two main signals of NO_3 which are NO^+, NO_2^+) are used as variables in the PMF input matrix. Fragments of sulfate and chloride are not included because they are not added to the chamber and the concentration is found to be negligible. The values and errors of the input matrix and minimum error (minErr) were generated by Tofware v3.3 in Igor Pro 8. The fragment contributions are calculated using the fragmentation table for terpene-related mixture (see Fig. S1).

We start the PMF analysis by varying the seed value (min = 0, max = 20, delta = 1) to pick different initial values for the PMF algorithm and choose the optimum number of factors (p). After choosing p and the seed value, the rotationality of the solution is explored by varying the rotation (f_{peak}) value (min = -1, max = +1, delta = 0.2). Lastly, bootstrapping runs are performed with 100 iterations to estimate the uncertainties in the factor profile and time series.

We choose a two-factor solution (see Fig. S2) because we are interested in splitting the aerosol mass only into pAmN and pON, and that low residuals and local minima (Q/Q_{exp}) have already been reached in this configuration (p = 2; seed = 0; f_{peak} = 0). The statistical summary of the PMF analysis is presented in Fig. S3. The time series of the measured total mass, the total reconstructed PMF mass, and the total residuals, as well as the scaled residuals of each factor m/z variable of the chosen PMF analysis are shown in Fig. S4. The chosen PMF solution split the total mass concentration into F1 and F2, representing the OA mixture and pAmN, respectively (see Fig. S2c-h). F1 has a factor profile with signals mainly from organic fragments, as well as ammonium and nitrate (Fig. S2c,e), which can be assumed to be particulate organic nitrate and amines. Meanwhile, F2 profile contains mainly signals from ammonium nitrate, with negligible background organic signals (Fig. S2d,f).

Since we add NO^+ and NO_2^+ to the input matrix, it is interesting to see that PMF is separating the two factors based on the $\text{NO}_2^+/\text{NO}^+$. We can determine R_{pAmN} from F2 (pAmN) by simply calculating $\text{NO}_2^+/\text{NO}^+$ = 0.0119 in the factor profile, which is close to the experimental value of R_{pAmN} = 0.0115. The same applies for R_{pON}, where we can use F1 (OA) that contains pON to determine R_{pON}, which is found to be $\text{NO}_2^+/\text{NO}^+$ = 0.0003, showing that the R_{pON} value is approaching zero as expected.

To validate the factor profiles, the time series of F1 and F2 (see Fig. S2g,h) are compared to the ACSM Org, NO_3, and NH_4 time series. The concentration of F2 is compared to the total concentration of pAmN (C_{pAmN}), which is the total concentration of NO_3 in pAmN ($C_{\text{NO}_3\text{,pAmN}}$, obtained from NO_x^+ ratio method) and an equimolar amount of NH_4 ($C_{\text{NH}_4\text{,pAmN}}$). The comparison suggests a good correlation between the two (r^2 = 0.98). Similarly, the concentration of F1 is compared to the total concentration of OA (C_{OA}), which is the total concentration of organic aerosol in the chamber, assumed as the sum of concentrations of total ACSM Org (C_{Org}), NO_3 in pON ($C_{\text{NO}_3\text{,pON}}$, obtained from NO_x^+ ratio method), and the excess NH_4 that has not been assigned to ammonium nitrate ($C_{\text{NH}_4\text{,excess}} = C_{\text{NH}_4\text{,total}} - C_{\text{NH}_4\text{,pAmN}}$), which is relatively small compared to the total ammonium. The comparison also shows a good correlation between the two (r^2 = 0.99).

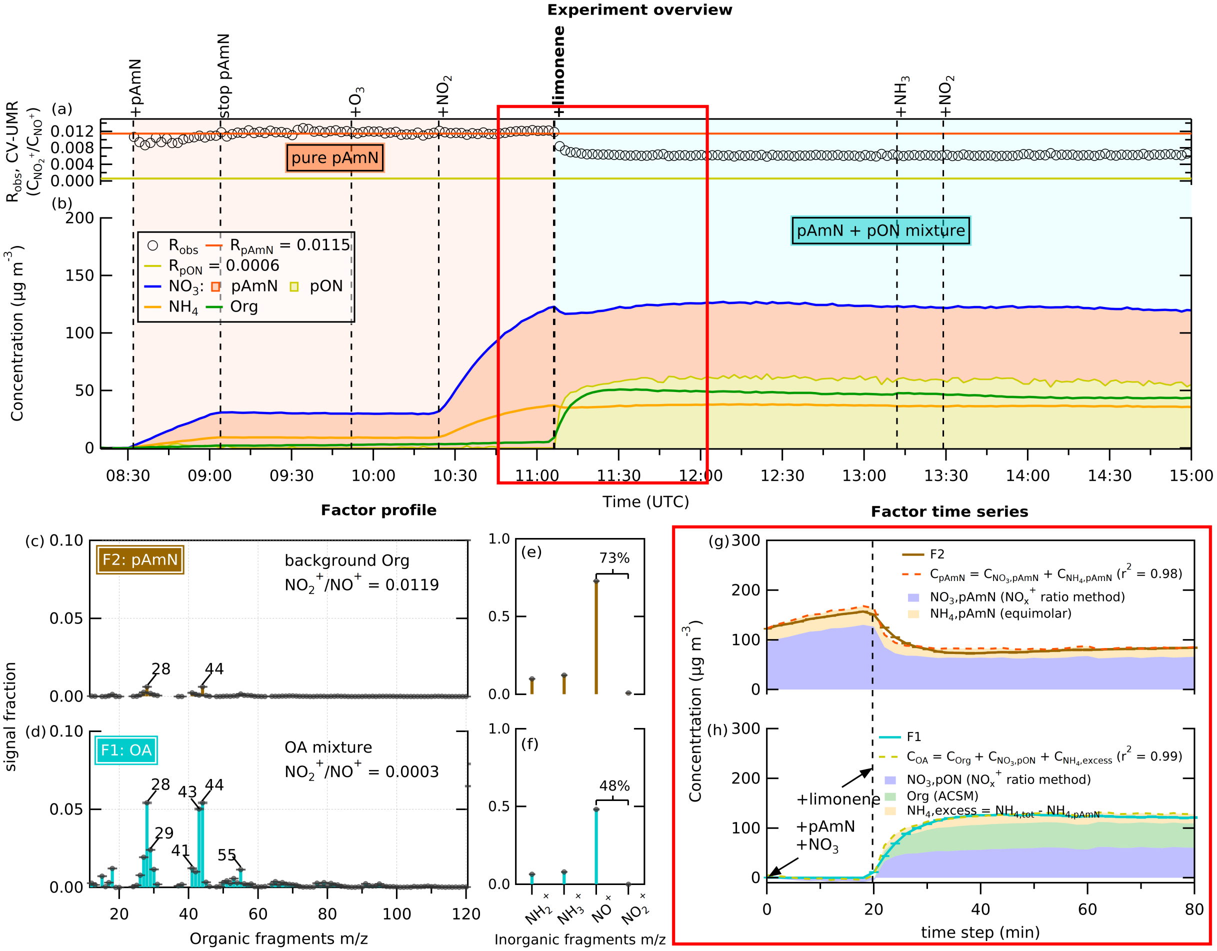

Figure S2. Overview of the PMF analysis of a chamber experiment using limonene precursor in AIDA chamber during CAINA campaign. Plot (a) shows the time series of R_{obs}, R_{pAmN}, and R_{pON} measured by CV-UMR-ToF-ACSM. Plot (b) shows the time series of ACSM species of $\mathrm{NO_3}$, $\mathrm{NH_4}$, Org, as well as the apportioned pON and pAmN stacked to fit the total $\mathrm{NO_3}$. The red square indicates the period where the PMF analysis is performed. Plots (c-h) show the two-factor solution of PMF analysis using Org fragments from m/z 12 to 120 and inorganic fragments ($\mathrm{NH_2^+}$ = NH4_16, $\mathrm{NH_3^+}$ = NH4_17, $\mathrm{NO^+}$ = NO3_30, and $\mathrm{NO_2^+}$ = NO3_46) as input matrix. Plots (c-f) describe the factor profiles with uncertainties from bootstrapping. F1 is shown to represent the OA mixture in the chamber, consisting of Org, nitrate, and amines ($\mathrm{NO_2^+/NO^+}$ = 0.0003), while F2 represents ammonium nitrate with negligible organic component ($\mathrm{NO_2^+/NO^+}$ = 0.0119). Plot (g) shows the factor time series where F2 is compared with the concentration of pAmN (C_{pAmN}). Plot (h) shows the factor time series where F1 is compared with the concentration of total OA (C_{OA}).

In order to be able to compare f_{pON} from the PMF analysis with other methods, we calculated f_{pON} from F1. Since $\mathrm{NO_3}$ fragments account for ∼48% of F1 profile, $C_{\mathrm{NO_3,pON}}$ will have such contribution to the concentration of F1. By taking the ratio of $C_{\mathrm{NO_3,pON}}$ to the total concentration of $\mathrm{NO_3}$, we can calculate f_{pON} from PMF. The comparison of f_{pON} obtained from PMF analysis and from $\mathrm{NO_x^+}$ ratio method (both CV-UMR-ToF-ACSM and SV-HR-ToF-AMS) can be seen in Fig. 8.

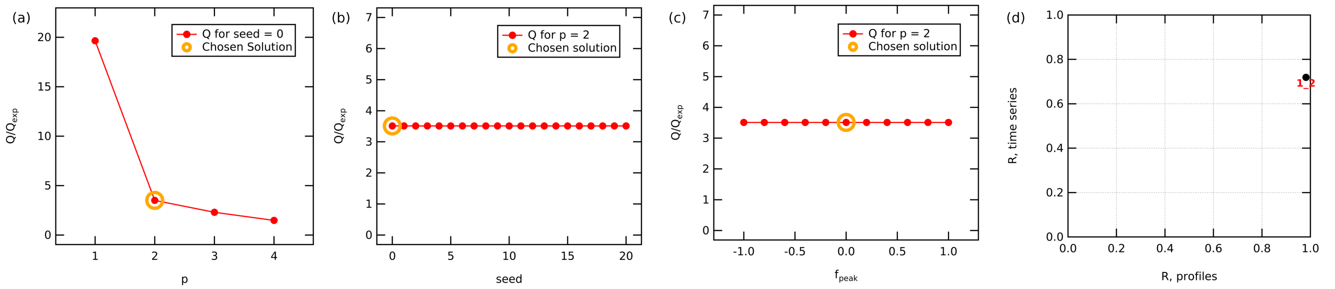

Figure S3. Diagnostic plots of PMF analysis showing (a) Q/Q_{exp} vs. number of factors (p), (b) Q/Q_{exp} vs. seed value, (c) Q/Q_{exp} vs. f_{peak} value, and (d) correlation of time series and mass spectra among two PMF factors (R time series vs. R profiles). The value of p = 2, seed = 0, and f_{peak} = 0 are chosen.

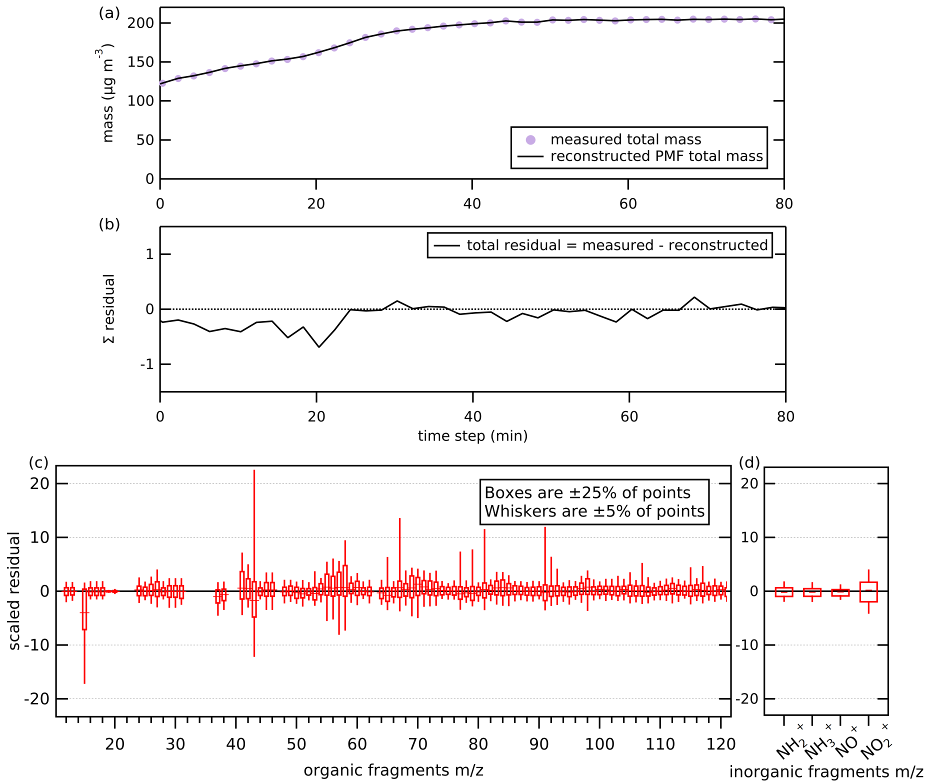

Figure S4. Diagnostic plots of the chosen PMF solution showing (a) time series of the measured total mass and reconstructed PMF mass, (b) time series of residual and scaled residual of the least-square-fit, (c) distribution of scaled residuals for each organic fragment m/z, and (d) distribution of scaled residuals for each inorganic fragment.

References

Allan, J. D., Delia, A. E., Coe, H., Bower, K. N., Alfarra, M., Jimenez, J. L., Middlebrook, A. M., Drewnick, F., Onasch, T. B., Canagaratna, M. R., Jayne, J. T., and Worsnop, D. R.: A generalised method for the extraction of chemically resolved mass spectra from Aerodyne aerosol mass spectrometer data, Journal of Aerosol Science, 35, 909–922, https://doi.org/10.1016/j.jaerosci.2004.02.007, 2004.

Bahreini, R., Ervens, B., Middlebrook, A. M., Warneke, C., De Gouw, J. A., DeCarlo, P. F., Jimenez, J. L., Brock, C. A., Neuman, J. A., Ryerson, T. B., Stark, H., Atlas, E., Brioude, J., Fried, A., Holloway, J. S., Peischl, J., Richter, D., Walega, J., Weibring, P., Wollny, A. G., and Fehsenfeld, F. C.: Organic aerosol formation in urban and industrial plumes near Houston and Dallas, Texas, Journal of Geophysical Research: Atmospheres, 114, 2008JD011 493, https://doi.org/10.1029/2008JD011493, 2009.

Carlton, A. G., De Gouw, J., Jimenez, J. L., Ambrose, J. L., Attwood, A. R., Brown, S., Baker, K. R., Brock, C., Cohen, R. C., Edgerton, S., Farkas, C. M., Farmer, D., Goldstein, A. H., Gratz, L., Guenther, A., Hunt, S., Jaeglé, L., Jaffe, D. A., Mak, J., McClure, C., Nenes, A., Nguyen, T. K., Pierce, J. R., De Sa, S., Selin, N. E., Shah, V., Shaw, S., Shepson, P. B., Song, S., Stutz, J., Surratt, J. D., Turpin, B. J., Warneke, C., Washenfelder, R. A., Wennberg, P. O., and Zhou, X.: Synthesis of the Southeast Atmosphere Studies: Investigating Fundamental Atmospheric Chemistry Questions, Bulletin of the American Meteorological Society, 99, 547–567, https://doi.org/10.1175/BAMS-D-16-0048.1, 2018.

Farmer, D. K., Matsunaga, A., Docherty, K. S., Surratt, J. D., Seinfeld, J. H., Ziemann, P. J., and Jimenez, J. L.: Response of an aerosol mass spectrometer to organonitrates and organosulfates and implications for atmospheric chemistry, Proceedings of the National Academy of Sciences, 107, 6670–6675, https://doi.org/10.1073/pnas.0912340107, 2010.

Fry, J. L., Brown, S. S., Middlebrook, A. M., Edwards, P. M., Campuzano-Jost, P., Day, D. A., Jimenez, J. L., Allen, H. M., Ryerson, T. B., Pollack, I., Graus, M., Warneke, C., de Gouw, J. A., Brock, C. A., Gilman, J., Lerner, B. M., Dubé, W. P., Liao, J., and Welti, A.: Secondary organic aerosol (SOA) yields from NO_3 radical + isoprene based on nighttime aircraft power plant plume transects, Atmospheric Chemistry and Physics, 18, 11 663–11 682, https://doi.org/10.5194/acp-18-11663-2018, 2018.

Hu, W., Handschy, A., and Jimenez, J. L.: AMS Capture Vaporizer Spectral Database, http://cires1.colorado.edu/jimenez-group/AMSsd_CV/, (last access: 9 July 2025), [dataset].

Hu, W., Campuzano-Jost, P., Day, D. A., Croteau, P., Canagaratna, M. R., Jayne, J. T., Worsnop, D. R., and Jimenez, J. L.: Evaluation of the new capture vaporizer for aerosol mass spectrometers (AMS) through field studies of inorganic species, Aerosol Science and Technology, 51, 735–754, https://doi.org/10.1080/02786826.2017.1296104, 2017.

Hu, W., Day, D. A., Campuzano-Jost, P., Nault, B. A., Park, T., Lee, T., Croteau, P., Canagaratna, M. R., Jayne, J. T., Worsnop, D. R., and Jimenez, J. L.: Evaluation of the new capture vaporizer for aerosol mass spectrometers: Characterization of organic aerosol mass spectra, Aerosol Science and Technology, 52, 725–739, https://doi.org/10.1080/02786826.2018.1454584, 2018a.

Hu, W., Day, D. A., Campuzano-Jost, P., Nault, B. A., Park, T., Lee, T., Croteau, P., Canagaratna, M. R., Jayne, J. T., Worsnop, D. R., and Jimenez, J. L.: Evaluation of the New Capture Vaporizer for Aerosol Mass Spectrometers (AMS): Elemental Composition and Source Apportionment of Organic Aerosols (OA), ACS Earth and Space Chemistry, 2, 410–421, https://doi.org/10.1021/acsearthspacechem.8b00002, 2018b.

Takeuchi, M. and Ng, N. L.: Chemical composition and hydrolysis of organic nitrate aerosol formed from hydroxyl and nitrate radical oxidation of α-pinene and β-pinene, Atmospheric Chemistry and Physics, 19, 12 749–12 766, https://doi.org/10.5194/acp-19-12749-2019, 2019.